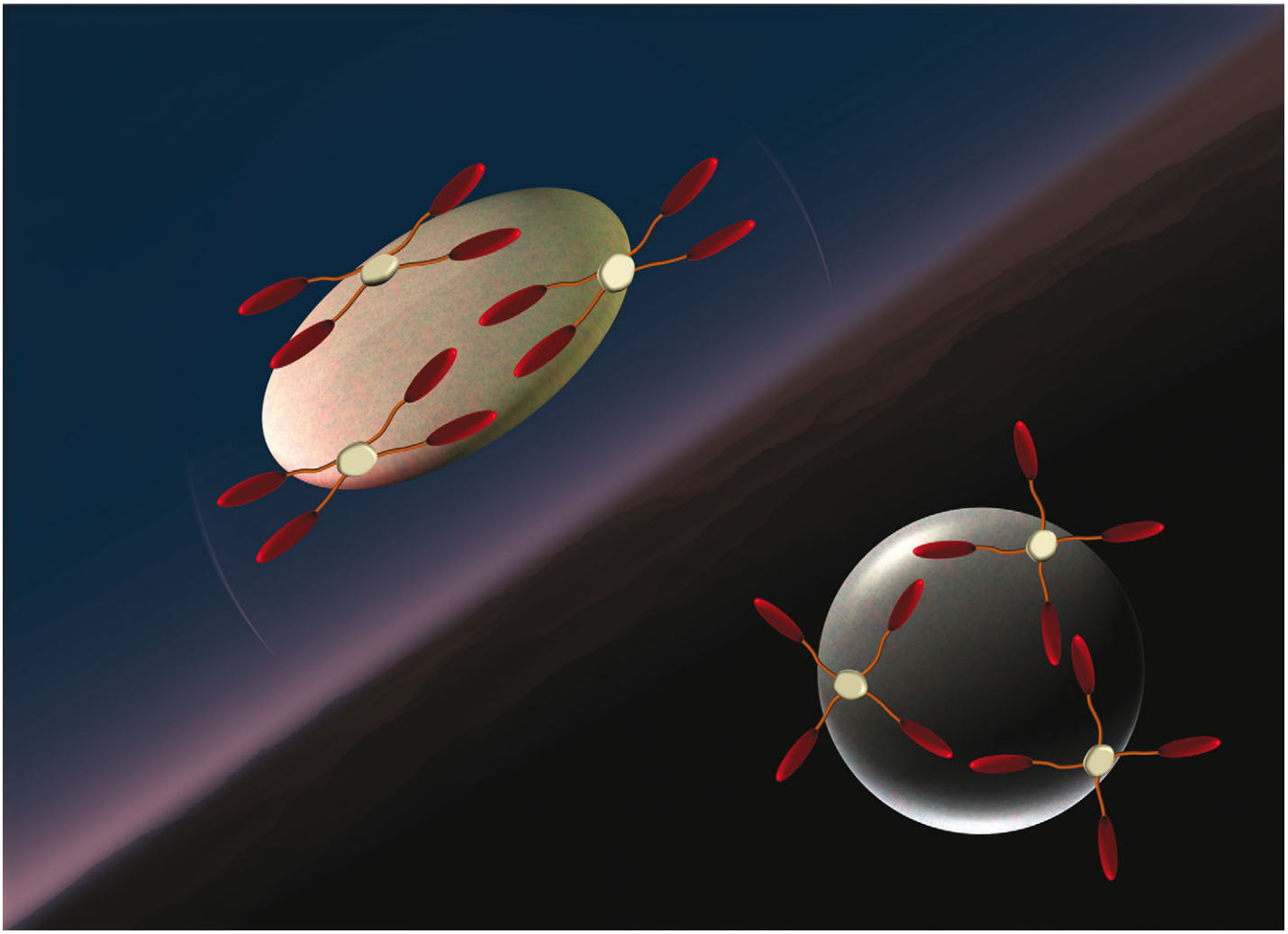

Highlighting collaborative research from Kwang-Un Jeong (Chonbuk National University) and Namil Kim (Korea Automotive Technology Institute), South Korea.

Optically isotropic liquid crystal media formulated by doping star-shaped cyclic oligosiloxane liquid crystal surfactants in twin nematic liquid crystals

Optically isotropic liquid crystal (LC) media have been formulated by doping star-shaped molecular surfactants (SiLC) into rod-shaped twin LC (DiLC) host molecules. The optically isotropic LC media can allow us to fabricate new electro-optical flexible devices without applying LC alignment layers.

As featured in:

See Kwang-Un Jeong *et al.*, *Soft Matter*, 2015, **11**, 3772.

ROYAL SOCIETY OF CHEMISTRY

www.softmatter.org

Registered charity number: 207890

Soft Matter

PAPER

Cite this: *Soft Matter*, 2015, **11**, 3772

Optically isotropic liquid crystal media formulated by doping star-shaped cyclic oligosiloxane liquid crystal surfactants in twin nematic liquid crystals†

Namil Kim,[b] Dae-Yoon Kim,[a] Minwook Park,[a] Yu-Jin Choi,[a] Soeun Kim,[a] Seung Hee Lee[c] and Kwang-Un Jeong*[a]

Received 2nd January 2015,
Accepted 5th March 2015

DOI: 10.1039/c5sm00005j

www.rsc.org/softmatter

The formation of optically isotropic liquid crystal (LC) media has been investigated by doping the star-shaped LC molecular surfactants (SiLC) into the rod-shaped twin LC host molecules (DiLC). The experimental phase diagram was constructed on the basis of differential scanning calorimetry (DSC) and then a theoretical calculation was conducted through a combined Flory–Huggins (FH)/Maier–Saupe–McMillan (MSM)/phase field (PF) model to account for the experimental results. The phase diagram of the SiLC/DiLC mixtures revealed the broad coexistence regions such as smectic A + crystal (SmA_1 + Cr_2), liquid + crystal (L_1 + Cr_2), and liquid + nematic (L_1 + N_2) at the intermediate composition along with the narrow single phase crystal (Cr_2), smectic (SmA_1), and nematic (N_2) regions. The morphologies and structures of these coexistence regions were further confirmed by polarized optical microscopy (POM) and wide-angle X-ray diffraction (WAXD). At the 80/20 SiLC/DiLC composition, the optical anisotropy was induced under an alternating current (AC) electric field above its isotropization temperature. The formation of an optically isotropic LC medium in mixtures of the SiLC molecular surfactants and nematic LC host may allow us to develop new electro-optical devices.

1. Introduction

Although liquid crystal display (LCD) technology has made rapid progress, there are still many obstacles to overcome. Fast response time, for instance, is one of the critical issues to achieve high image resolution and colour sequential operation. Electro-optical switching performance can be partially improved with the aid of an external electric field, referred to as the Kerr effect.[1–6] The Kerr effect is driven in the optically isotropic phase by the reorientation of polar molecules under an electric field, accompanying large changes in the optical properties. In general, a large Kerr effect is observed in the isotropic phase slightly above the nematic (N)–isotropic (I) transition temperature (T_{NI}) of LC molecules, where the correlated molecules have a nematic-like molecular orientational order on a length scale defined by a coherent length. The electro-optical properties of the nematic LC (NLC) are very sensitive to temperature. An optically isotropic blue phase formed between the helical cholesteric phase and the isotropic phase also becomes anisotropic when a strong field is applied.[7–13] Compared to the conventional vertical alignment (VA) and in-plane switching (IPS) LC modes, it exhibits wide viewing angle and cell gap insensitivity along with alignment-layer free processibility.[14–16] However, the blue phase appears in a very narrow temperature range (~2 °C) and thus the application area is limited. In this regard, a polymer network is employed to stabilize the blue phase, the so-called polymer-stabilized blue phase (PSBP).

The NLC microemulsion system consisting of water, the amphiphilic surfactant, and anisotropic LC has received much attention because of its unusual phase behavior.[17–20] When the nanometer-sized water droplets are uniformly dispersed within a LC medium, an optically isotropic LC phase appears prior to undergoing phase separation. The mixtures are optically transparent on a macroscopic scale, but they still possess the local molecular orientational order. Therefore, the isotropic phase in a microemulsion system is expected to exhibit a large Kerr effect. However, the size of water particles and their uniform distribution in the NLC host medium are difficult to regulate because of the weak interactions between the water droplets and NLC molecules.

To challenge these drawbacks, we formed the optically isotropic LC phase by doping the star-shaped LC molecular

[a] *Department of Polymer-Nano Science and Technology, Chonbuk National University, Jeonju, Jeonbuk, 561-756, Korea. E-mail: kujeong@jbnu.ac.kr*
[b] *Smart Materials R&D Center, Korea Automotive Technology Institute, Cheonan, Chungnam 330-912, Korea*
[c] *Department of BIN Fusion Technology, Chonbuk National University, Jeonju, 561-756, Korea*

† Electronic supplementary information (ESI) available: Detailed experimental procedures. See DOI: 10.1039/c5sm00005j

surfactants (SiLC) into the rod-like twin LC (DiLC) host medium. Here, the SiLC molecular surfactant was synthesized by covalently linking four cyanobiphenyl anisotropic mesogens to the periphery of a super-hydrophobic and flexible cyclic tetramethyltetrasiloxane ring with hexyl connectors. The detailed synthetic route and its chemical characterization were demonstrated in our previous paper.[21] The SiLC molecules exhibited the phase transition from the smectic A (SmA) phase to the isotropic (I) phase. There is a strong phase separation between the cyclic oligosiloxane rings and the cyanobiphenyl anisotropic mesogens even above the isotropization temperature. Therefore, the SiLC with the dimension of 4.2 nm in length and 1.3 nm in width may break down into the macroscopic NLC domains of the DiLC compound. The host DiLC molecule was synthesized by chemically linking two cyanobiphenyl mesogens with a dodecyl flexible connector. Since both SiLC and DiLC contain cyanobiphenyl mesogens, the guest SiLC molecular surfactants may not be macroscopically phase-separated from the host DiLC molecule and effectively disrupt the formation of the N domains. The experimental phase diagram of the SiLC/DiLC mixtures was first established based on the differential scanning calorimetry (DSC), polarized optical microscopy (POM) and wide angle X-ray diffraction (WAXD) results. The phase behavior was clarified by conducting the theoretical calculation through the combination of Flory–Huggins (FH), Maier–Saupe–McMillan (MSM), and phase field (PF) models. The electric field-induced optical anisotropy of the mixture was investigated in the vicinity of the isotropization temperature. Transmittance and morphological changes were monitored as a function of the temperature and operating voltage.

2. Experimental

Materials

4′-Hydroxy-4-biphenylcarbonitrile (97%, Aldrich), 1,12-dibromododecane (98%, Aldrich) and potassium carbonate (K_2CO_3, 99.99%, Aldrich) were used as-received. *N*,*N*-Dimethylformamide (DMF, 99.8%, Sigma-Aldrich) was distilled by the conventional method prior to use. Merck silica gel (9385 grade, 230–400 mesh) was used for column chromatography separations.

Synthesis of SiLC

The synthetic scheme and chemical structure of a star-shaped molecule consisting of a 2,4,6,8-tetramethyl-cyclotetrasiloxane with 4′-hydroxy-4-biphenylcarbonitrile were described well in the literature.[21] ^{1}H NMR (400 MHz, $CDCl_3$, TMS): δ = 0.08 (s, 12H), 0.55 (t, 8H), 1.40 (m, 24H), 1.79 (m, 8H), 3.98 (t, 8H), 6.96 (m, 8H), 7.49 (m, 8H), 7.60 (m, 8H), 7.67 ppm (m, 8H).

Synthesis of DiLC

1,12-Di(4-cyano-4′-biphenoxy)dodecane (DiLC) (yield: 74%, 2.12 g) was synthesized by the reaction of 4-cyano-4′-hydroxybiphenyl (2.53 g, 12.95 mmol) with 1,12-dibromododecane (1.70 g, 5.18 mmol) in the presence of the K_2CO_3 (2.65 g, 13.60 mmol) catalyst (Fig. S1†). ^{1}H NMR (400 MHz, $CDCl_3$, TMS): δ = 1.31 (m, 12H), 1.47 (m, 4H), 1.81 (m, 4H), 4.0 (t, 4H), 7.0 (d, 4H), 7.5 (d, 4H), 7.60–7.70 (q, 8H).

Sample preparation and characterization

The mixtures of various SiLC/DiLC compositions were heated slowly until the respective constituents were melted completely and then mechanically stirred to become homogenous. The samples were cooled down and finely ground for the thermal, optical and structural analyses. Phase transition temperatures of neat DiLC and SiLC/DiLC mixtures were determined using differential scanning calorimetry (DSC, Perkin-Elmer PYRIS Diamond) with an Intracooler 2P apparatus. The sample of approximately 5.0 mg was sealed into an aluminium hermetic pan, where the weight of the empty pan was kept constant with a precision of $\pm$0.001 mg. The temperature and heat flow were calibrated at various heating and cooling rates. The cooling scan always preceded the heating scan at the same rate in order to eliminate the thermal histories.

For one-dimensional (1D) wide-angle X-ray diffraction (WAXD) measurements, a thin film with a thickness of about 1 mm was prepared by melting the sample on an aluminium plate. The 1D WAXD experiments were conducted in the reflection mode of a Rigaku 12 kW rotating-anode X-ray (Cu Kα radiation) generator. Diffraction positions and widths were calibrated using silicon crystals in the high 2θ-angle region ($>15^\circ$) and silver behenate in the low 2θ-angle region. A hot stage was coupled to the diffractometer to monitor the temperature-dependent structural evolution.

Temperature-dependent texture changes were examined using cross-polarized optical microscopy (POM, Nikon ECLIPSE LV100POL) equipped with a heating stage (METTLER TOLEDO FP90 Central Processor). The temperature and cooling/heating rates were calibrated with an accuracy of $\pm$0.5 °C and $\pm$0.05 °C min^{-1}, respectively. The samples were melt-processed between two bare cover glasses with a thickness of approximately 10 μm. The samples were heated to an optically isotropic state and then cooled at 1.0 °C min^{-1}.

The electro-optical switching performance of the SiLC/DiLC mixtures was monitored in the in-plane switching (IPS) cell with respect to the temperature and intensity of an electric field. The electric field with an alternating current (AC) voltage (60 Hz) was applied using a waveform generator (Tektronix, AFG 3022, USA). Transmittance at an 'on' and 'off' state has been recorded. The IPS LC test cell contained an interdigitated common and signal electrode on the bottom substrate. The cell gap (d), width (w), and distance (l) of the electrode were controlled to be 10 $\pm$ 0.01, 4.0 and 4.0 μm, respectively.

The Model description

A theoretical phase diagram of the mixtures exhibiting the crystal (Cr), smectic A (SmA), and nematic (N) phases has been established by employing a combined Flory–Huggins (f^{FH}), Maier–Saupe/Maier–Saupe–McMillan ($f^{MS/MSM}$), and phase field (f^{PF}) model, that is, $f = f^{FH} + f^{MS/MSM} + f^{PF}$.[22] In the Flory–Huggins theory, the enthalpic and entropic changes on mixing are derived in the context of the statistical lattice model where the respective constituents occupy a lattice with no specific interactions. The Maier–Saupe theory is based on a

mean field approximation. The energy of rigid-rod molecules is independent of its particular environment. An additional order parameter characterizing the layered structure in the smectic phase was introduced by McMillan to demonstrate smectic–nematic or smectic–isotropic transitions. Solidification behavior such as crystallization can be explained by the phase field model in which the state of the entire structure may be represented continuously by the crystal order parameter.

The free energy density of liquid–liquid demixing is commonly described using the Flory–Huggins (FH) theory,[23,24]

$$f^{\mathrm{FH}} = \frac{\phi_1}{r_1}\mathrm{In}\,\phi_1 + \frac{\phi_2}{r_2}\mathrm{In}\,\phi_2 + \chi_{\mathrm{aa}}\phi_1\phi_2 \quad (1)$$

where r_1 and r_2 represent the numbers of the lattice sites occupied by components 1 and 2. The volume fractions (ϕ_1, ϕ_2) are given by $\phi_1 = n_1r_1/n_1r_1 + n_2r_2$ and $\phi_2 = n_2r_2/n_1r_1 + n_2r_2$, where n_1 and n_2 are the numbers of the respective molecules. The amorphous–amorphous interaction parameter, χ_{aa}, is inversely proportional to the absolute temperature, assumed by $\chi_{\mathrm{aa}} = A + B/T$, in which A and B are constants.

The free energy density of N and SmA ordering can be expressed by a combined Maier–Saupe (MS) and Maier–Saupe–McMillan (MSM) theory.[25–28]

$$f^{\mathrm{MS/MSM}} = -\sum_1 \phi_1 - \sum_2 \phi_2 - \frac{1}{2}v_{11}\left(s_1{}^2 + \alpha_1\sigma_1{}^2\right)\phi_1{}^2 - \frac{1}{2}v_{22}s_2{}^2\phi_2{}^2 - v_{12}s_1s_2\phi_1\phi_2 \quad (2)$$

The first two terms mean the decreases of entropy due to the anisotropic long-range ordering, while the last three terms correspond to the enthalpic contributions arising from the alignment of LC directors. The cross-interaction parameter may be determined by the interaction parameter of the pure components, *i.e.*, $v_{12} = c\sqrt{v_{11}v_{22}}$, where c is the proportional constant characterizing the relative strength between the dissimilar mesogens. The value α_1 representing the dimensionless interaction strength for the smectic ordering provides the phase transformation information, that is, the SmA–N phase transition at $0.7 < \alpha_1 < 0.98$ and SmA–I transition at $\alpha_1 > 0.98$. The smectic order parameter may be coupled with the nematic interaction parameter by,

$$v_{11}\alpha_1 = 4.541\frac{T_{\mathrm{SI}}}{T} \quad (3)$$

The entropic term can be described in detail as,

$$\sum_j = -\iint f(z, \cos\theta_j)\mathrm{In}\left[4\pi f(z, \cos\theta_j)\right]\mathrm{d}z\mathrm{d}\Omega_j = \mathrm{In}\,Z_j - m_{\mathrm{n},j}s_j - m_{\mathrm{s},j}\sigma_j \quad (4)$$

where $m_{\mathrm{n},j}$ and $m_{\mathrm{s},j}$ are the dimensionless nematic and smectic mean field parameters. The orientation distribution function, $f(z, \cos\theta_j)$, and partition function, Z, can be expressed as follows.

$$f(z, \cos\theta_j) = \frac{1}{4\pi Z_j}\exp\left[\frac{1}{2}m_{\mathrm{n},j}\left(3\cos^2\theta_j - 1\right)\right] \times \exp\left[\frac{1}{2}m_{\mathrm{s},j}\cos\left(2\pi z/d_j\right)\left(3\cos^2\theta_j - 1\right)\right] \quad (5)$$

$$Z_j = \iint \exp\left[\frac{1}{2}m_{\mathrm{n},j}\left(3\cos^2\theta_j - 1\right)\right] \times \exp\left[\frac{1}{2}m_{\mathrm{s},j}\cos\left(2\pi z/d_j\right) \times \left(3\cos^2\theta_j - 1\right)\right]\mathrm{d}z\mathrm{d}\Omega_j \quad (6)$$

The nematic (s_j) and smectic (σ_j) order parameters are defined as,

$$s_j = \frac{1}{2}\left\langle 3\cos^2\theta_j - 1\right\rangle \quad (7)$$

$$\sigma_j = \frac{1}{2}\left\langle\cos\left(2\pi z/d_j\right)\left(3\cos^2\theta_j - 1\right)\right\rangle \quad (8)$$

The free energy density of crystal solidification can be expressed by the phase field model in which the free energy of a pure crystal has a Landau-type asymmetric double-well with respect to the crystal order parameter (ψ).[29,30]

$$f\left(\psi_j\right) = \frac{F\left(\psi_j\right)}{k_{\mathrm{B}}T} = W_j\int_0^{\psi_j}\psi_j\left(\psi_j - \zeta_j\right)\left(\psi_j - \zeta_{j,0}\right)\mathrm{d}\psi_j = W_j\left[\frac{\zeta_j(T)\zeta_{j,0}\left(T_{j,\mathrm{m}}\right)}{2}\psi_j{}^2 - \frac{\zeta_i(T) + \zeta_{j,0}\left(T_{j,\mathrm{m}}\right)}{3}\psi_j{}^3 + \frac{1}{4}\psi_j{}^4\right] \quad (9)$$

The third order coefficient should be a finite value to describe the first order phase transition. The crystalline order parameter at the solidification potential for crystallization, $\zeta_{i,0}$, is taken as unity for small molecules. The coefficient W_i, indicating the energy barrier for the crystal nucleation to overcome, can be estimated experimentally from the melting point ($T^{\mathrm{o}}_{i,\mathrm{m}}$) and heat of fusion ($\Delta H^{\mathrm{u}}_i$), that is, $W_i = 6\Delta H^{\mathrm{u}}_i/RT(1 - T/T^{\mathrm{o}}_{i,\mathrm{m}})(\zeta_{i,0}/2 - \zeta_i)^{-1}$. From the total free energy curve obtained at various temperatures, the coexistence points are determined by balancing the chemical potentials for each phase.[31]

3. Results and discussion

Phase transition behaviors of neat SiLC and DiLC

Fig. 1 summarizes the phase transition behavior of neat SiLC. Four cyanobiphenyl anisotropic mesogens are chemically connected to the periphery of a super-hydrophobic and ultra-flexible cyclic tetramethyltetrasiloxane ring, where the number of methylene linkages is six. The SiLC molecular surfactants exhibit the SmA phase by the self-organization of rigid cyanobiphenyl mesogens in the nanophase separated domains and the monotropic phase transition to a crystalline (Cr) phase. During the heating process at 2.5 and 5 °C min^{-1}, crystallization occurs just above the glass transition temperature (T_{g} = 22 °C) and then the crystals are melted at 41 °C. Upon heating at 10 and 20 °C min^{-1}, the metastable glassy SmA phase

directly transforms to the stable SmA phase above the T_g and the I phase at 119 °C. During the cooling process, the I phase transforms to the SmA phase. Regardless of heating or cooling rates, the SmA–I transition is observed. Since the I ↔ LC transition is close to the equilibrium state, the transition temperature and its heat change are independent of the cooling and heating rates. Upon further lowering the temperature below the T_g, the symmetry and order of the smectic LC phase are retained to be a glassy smectic LC phase where the molecular mobility is restricted. On subsequent heating above the T_g, the metastable glassy SmA phase transforms to the stable Cr phase. The detailed monotropic phase transition behavior of SiLC surfactants were reported in our previous research.[21]

In the mixed state, it is expected that the DiLC molecule containing two cyanobiphenyl mesogens preferentially anchors on the SiLC molecular surfactants due to the favorable intermolecular interactions between the cyanobiphenyl mesogens attached both to SiLC and to DiLC. Therefore, the DiLC molecules may bridge the SiLC molecular surfactants, which subsequently lead to the formation of the optically isotropic medium. Note that the phase transition behaviors of LC dimers mainly depend on the length and relative position of the spacers.[32–34] The DSC thermograms of the as-synthesized DiLC molecules are depicted in Fig. 2a. Although the transition peaks and their intensities are affected by the scanning rates, the dual first-order thermal transitions are commonly observed. Upon heating, neat DiLC exhibits the major and minor endothermic peaks at 153 °C and 167 °C, while the dual exothermic peaks appear at 125 °C and 165 °C upon subsequent cooling. The temperature-dependent texture change is shown in the inset of Fig. 2a. On heating above 155 °C, the crystalline texture at 30 °C transforms to the schlieren texture with line disclination, which is a typical characteristic of the N phase. The image becomes completely dark upon further heating above 168 °C due to the isotropic melt. Therefore, the dual thermal transitions of DSC thermograms are the consequences of Cr–N and N–I transitions. It should be noted that the neat hexyloxy cyanobiphenyl mesogens (6OCB) reveals Cr–N and N–I transitions at around 57 °C and 76 °C, respectively.[35]

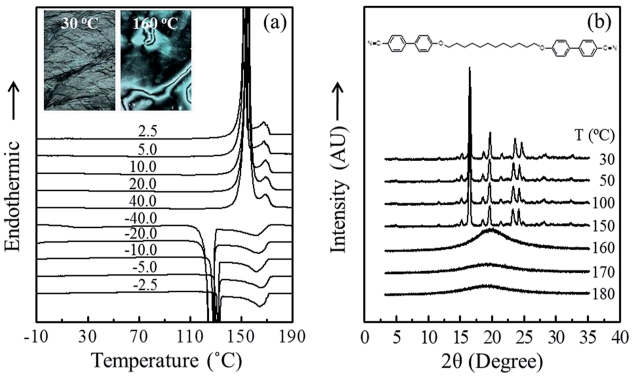

Fig. 2 (a) DSC thermograms of neat DiLC obtained at various scanning rates of 2.5, 5, 10, 20 and 40 °C min^{-1}, and (b) a set of 1D WAXD patterns taken at a heating rate of 2.5 °C min^{-1}.

Fig. 2b depicts the 1D WAXD patterns of neat DiLC at different temperatures. Four distinct diffraction peaks at 2θ = 16.5° (corresponding to the *d*-spacing of 0.537 nm), 19.7° (0.450 nm), 23.6° (0.376 nm), and 24.2° (0.367 nm) along with several minor peaks are clearly discerned at 30 °C. This result clearly indicates that the DiLC is highly ordered. No noticeable change is observed upon increasing the temperature up to 150 °C. On heating above 160 °C, all diffraction peaks abruptly disappeared, exhibiting a broad halo at 2θ = 20°. It implies that the crystal (Cr) phase transforms to a LC phase. Upon heating above 170 °C, the diffuse peak at 2θ = 20° shifts to a lower angle with reduced intensity due to the N to I transition even though the 1D WAXD patterns of the N and I phases are often indistinguishable. Based on the combined experimental results of DSC, POM, and WAXD, it is obvious that neat DiLC undergoes Cr–N–I transitions.

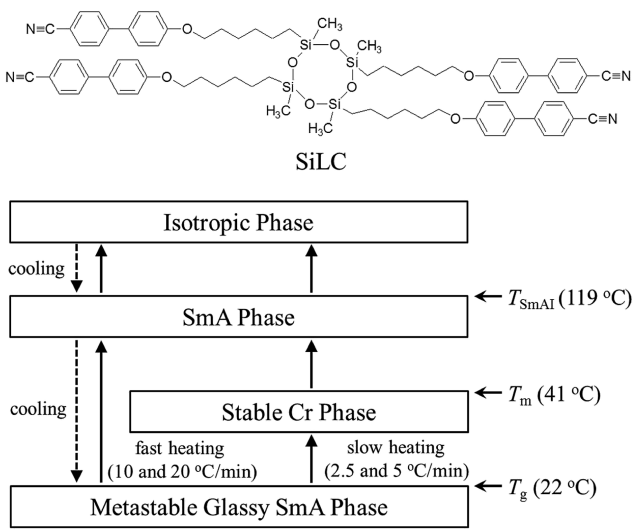

Fig. 1 The chemical structure and phase transition behavior of neat SiLC upon cooling and subsequent heating.

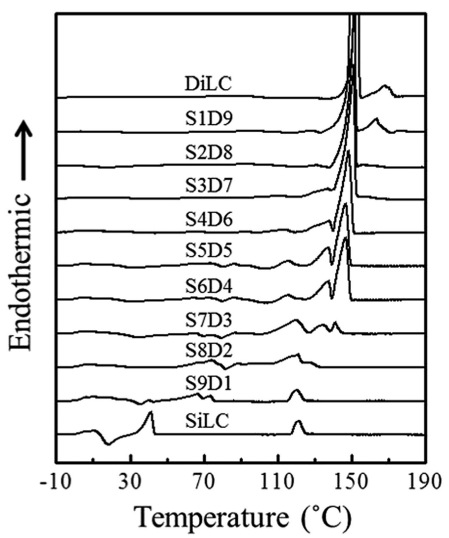

Fig. 3 DSC thermograms of SiLC/DiLC mixtures obtained at a heating rate of 2.5 °C min^{-1}, showing a gradual depression of the characteristic transition temperatures of the neat constituents in a mixed state.

Phase transition behaviors of SiLC/DiLC mixtures

The effect of the SiLC/DiLC blending ratio on phase transition temperatures has been investigated at a heating rate of 2.5 °C min^{-1}. The mixtures at various compositions are simplified by denoting S for SiLC and D for DiLC. The S5D5 symbol, for instance, represents that the mixture consists of 50 wt% of SiLC and 50 wt% of DiLC. As shown in Fig. 3, the characteristic endothermic thermal transitions of neat DiLC detected at 153 °C and 167 °C slightly shift to lower temperatures upon increasing the SiLC content and concurrently the peak intensity becomes weaker because of the plasticizing effect. A similar behavior is observed for the SmA–I transition of neat SiLC, but with a lower extent of depression. The transition temperature of SiLC at 119 °C is reduced to 117 °C at $<$60 wt% SiLC.

The effect of scanning rates on phase transition temperatures has been examined by gradually increasing from 2.5 to 40 °C min^{-1}.[36–39] The DSC thermograms of the 40/60 SiLC/DiLC mixture are displayed in Fig. 4. The strong endothermic transition close to 150 °C shifts to lower temperatures upon decreasing the heating rate, *i.e.*, from 153 °C at 40 °C min^{-1} to 149 °C at 2.5 °C min^{-1}, while the major exothermic peak associated with crystallization in the temperature range of 90–130 °C occurs at higher temperatures when cooled slowly. Generally, a higher degree of crystallinity is observed at slower cooling rates. The same experiments have been conducted over the entire blending compositions.

The characteristic transition temperatures corresponding to a pseudo-equilibrium state can be estimated by extrapolating the transition points determined at various heating rates to the zero heating rate. The variation of the Cr–N (T_{CrN}) and N–I (T_{NI}) transition temperatures of the neat DiLC is illustrated in the ESI (Fig. S2†). The equilibrium of the Cr–N and N–I transitions corresponding to the zero heating rate are predicted to be 153 °C and 167 °C, respectively, which are more than 5 °C lower than those determined at 40 °C min^{-1} ($T_{CrN,2}$ = 158 °C and $T_{NI,2}$ = 173 °C). The estimated transition temperature and corresponding heat of fusion are used as the material parameters for the theoretical calculation. Since DSC analysis alone is not enough to provide the complete phase behavior of the mixtures, we further conduct the numerical calculation, optical microscopy, and X-ray diffraction analyses.

The predictive capability of the theoretical calculation has been confirmed by comparing with the equilibrium transition points determined by extrapolating the DSC results. Although a hierarchical crystalline superstructure is developed during slow heating at a temperature slightly above the T_g, it is not taken into account for calculation because of its non-equilibrium nature. The material parameters used for calculation are thus $r_1 = 5$, $r_2 = 2$, $A = 0.2$, $T_c = -100$ °C, $\chi_{aa} = 0.39$ at $T = 160$ °C, $c_v = 0.8$, $\Delta H_2^u = 17$ kJ mol^{-1} at $T_{CrN,2} = 153$ °C, $T_{SmAI,1} = 119$ °C, and $T_{NI,2} = 167$ °C. The theoretical phase diagram is fitted with the DSC results by adjusting the strength of the cross-interaction and critical temperature. The SiLC constituent has only a smectic–isotropic transition and thus the α_1 value is chosen to be 1.07. The weak cross interaction signifies that the mixtures reveal the broad coexistence regions. The effect of cross-interaction and critical temperature on the phase diagram of mesogenic mixtures is thoroughly described in the literature.[28] Crystalline–amorphous interaction is closely associated with the melting point depression of the crystalline constituent.[40] The free energy curves of the FH/MSM/PF theory are plotted at various temperatures and then the coexistence lines are determined by minimizing the total free energy curve with respect to the volume fraction of each constituent. A single well representing isotropic mixture changes to a double well upon reducing the temperature due to the presence of coexistence regions. Fig. 5 shows the experimental and theoretical phase diagram of the SiLC/DiLC mixtures. The liquidus and solidus lines obtained by the theoretical calculation (solid lines) describe well the experimental transition points (as denoted by the

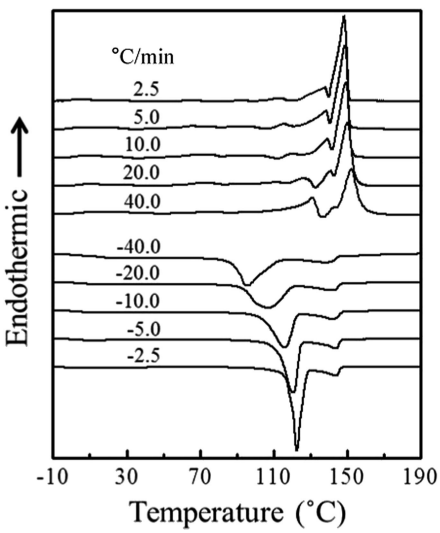

Fig. 4 DSC thermograms of the 40/60 SiLC/DiLC mixture obtained at various scanning rates ranging from 2.5 to 40 °C min^{-1}.

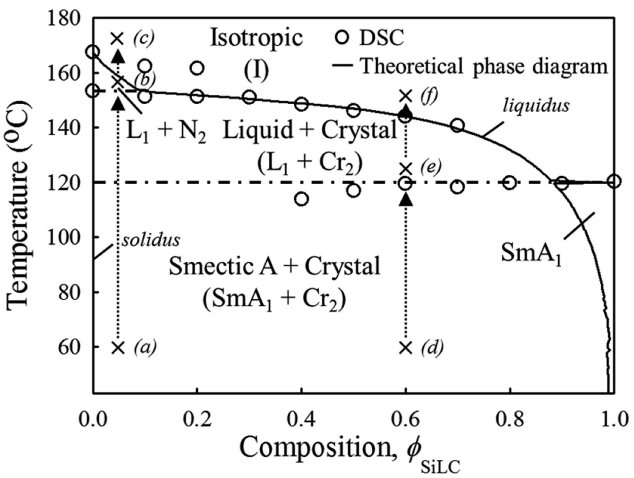

Fig. 5 The experimental (denoted by 'O') and theoretical (solid line) phase diagram of SiLC/DiLC mixtures, revealing the smectic A + crystal ($SmA_1 + Cr_2$), liquid + crystal ($L_1 + Cr_2$), and liquid + nematic ($L_1 + N_2$) coexistent regions along with the narrow crystal (Cr_1, Cr_2) and smectic A (SmA_1) regions.

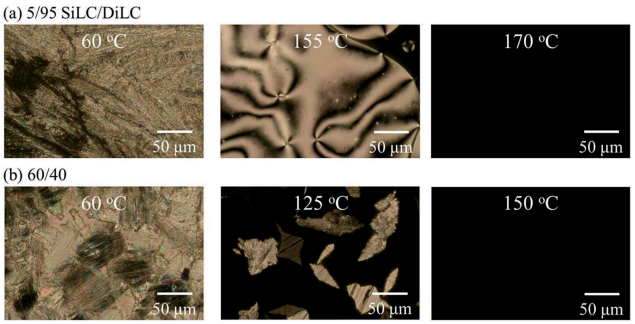

Fig. 6 Optical micrographs of the (a) 5/95 and (b) 60/40 SiLC/DiLC mixtures taken at a heating rate of 2.5 °C min^{-1}, showing the phase transformations upon elevating the temperature.

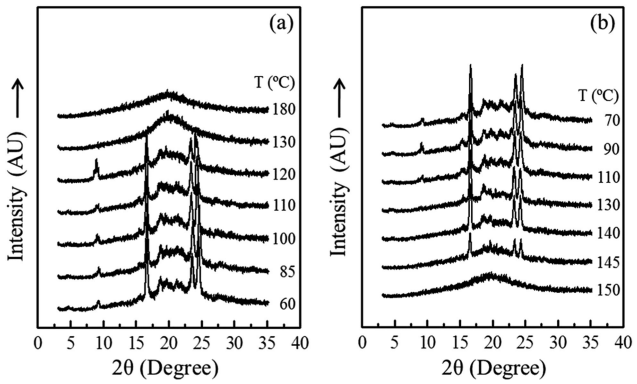

Fig. 7 A set of 1D WAXD powder patterns of the 60/40 SiLC/DiLC mixture obtained during a course of (a) cooling and (b) heating in the temperature range of 60–180 °C. The heating and cooling rates are maintained at 2.5 °C min^{-1}.

circular symbol) and additionally elucidate the phase boundary of the single and coexistence regions. Various coexistence regions such as the liquid + nematic (L_1 + N_2), liquid + crystal (L_1 + Cr_2), and smectic A + crystal (SmA_1 + Cr_2) are clearly discerned over the broad intermediate composition in a descending order of temperature. The single phase smectic A (SmA_1) appears at the extreme SiLC composition (>90 wt%) below 119 °C, while the single phase crystal (Cr_2) and nematic (N_2) regions from DiLC are difficult to identify in the phase diagram because the solidus line of the coexistent regions is located close to the axis of the neat DiLC. Although the mixtures are easily phase-separated upon cooling, the 6OCB in SiLC are expected to induce a strong interaction with the DiLC in a molecular level.

Optical micrographs of the mixtures acquired at a heating rate of 2.5 °C min^{-1} are shown in Fig. 6. All POM images are taken at a magnification of ×200. At the 5/95 SiLC/DiLC composition, the Cr domain covers the whole area at 60 °C, indicating that the DiLC crystals dominate the morphology (Fig. 6a). The Cr morphology transforms to the N phase at 155 °C and then to the I phase at 170 °C, respectively. According to the POM image at 155 °C, the dark area is identifiable at the edge of the schlieren texture and thus the isotropic liquid phase coexists with the N phase (corresponding to the L_1 + N_2 coexistence region). At the 60/40 SiLC/DiLC composition, the fan-shaped textures representing the SmA phase are not clearly discernible at 60 °C because of the competitiveness with the DiLC crystals (Fig. 6b). Upon heating above 120 °C, the optically isotropic area covers more than half of the microscopic area while maintaining the Cr domains. Since the SiLC constituent melts at around 119 °C, this region corresponds to the L_1 + Cr_2 coexistent region. Upon further heating to 150 °C, the DiLC crystals also melt into the I phase.

A set of 1D WAXD patterns of the 60/40 SiLC/DiLC mixture is shown in Fig. 7. During the cooling process, several diffraction peaks at 2θ = 8.9° (corresponding to the *d*-spacing of 0.992 nm), 16.6° (0.533 nm), 23.3° (0.381 nm), and 24.1° (0.369 nm) start to appear at 120 °C due to the development of a highly ordered structure. The peaks at 2θ = 16.6°, 23.3° and 24.1° are ascribed to the DiLC crystal. Similar diffraction patterns are still observed upon lowering the temperature below 60 °C (Fig. 7a). On subsequent heating to 130 °C, a small peak at 2θ = 8.9° disappears first presumably due to the SmA–I transition from SiLC (Fig. 7b). When the temperature reaches 150 °C the residual peaks disappear completely, revealing only an amorphous halo at around 2θ = 19.1°. According to the constructed phase diagram, the isotropization temperature at the 60/40 SiLC/DiLC composition occurs at around 144 °C. Morphological and structural observations describe well the various coexistent regions in the phase diagram.

Electric field-induced optical anisotropy

The effect of an AC electric field on the optical properties has been explored using the IPS LC test cell. Guided by the constructed phase diagram, the mixture having different blending ratios is heated slightly above its isotropization temperature. As the temperature decreases, transmittance increases from zero in the I state due to the emergence of cloudy or anisotropic domains from the LC phase. Fig. 8a shows the variation of the transmittance of the 80/20 SiLC/DiLC mixture when an electric field of 12.5 V μm^{-1} is applied. Under a zero electric field (symbolized by '□'), the transmittance increases all of a sudden from 0 to 17 at around 120 °C and then exhibits a gradual increment upon cooling up to 114 °C. Below 114 °C, the transmittance is almost levelled off in the range of 40–50, indicating that the anisotropic domains are fully developed. The phase transition temperature observed here is consistent with the DSC result. At the field-on state ('●'), on the other hand, the optical anisotropy takes place at 120.5 °C, about 0.5 °C higher than that of the zero electric field. A subtle difference occurring in optical anisotropy at an 'on' and 'off' state is indicated by the dotted area. The POM observation clearly shows the difference in the optical properties. The optically isotropic state at 120.5 °C transforms to the anisotropic state when an AC electric field is applied, as confirmed by the appearance of bright spots over the whole area (Fig. 8b). It is attributable to the development of the optically isotropic medium in a macroscopic region.

Fig. 9 displays the voltage-dependent transmittance curves measured at several temperatures. At 120.6 °C (square symbols) and 120.7 °C (circles), the induced birefringence is approximately proportional to the operating voltage. The cyanobiphenyl mesogens in SiLC and DiLC may be sensitive for the reorientation

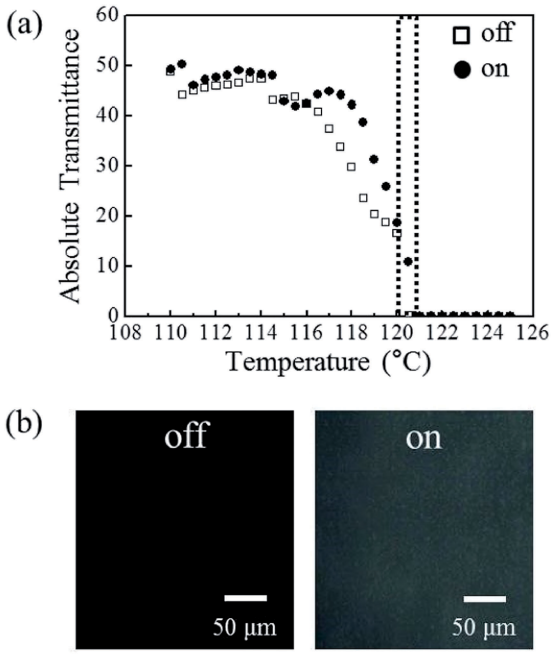

Fig. 8 Variation of the (a) transmittance and (b) optical micrographs of the 80/20 SiLC/DiLC mixture under the constant AC electric field of 12.5 V μm^{-1}. The occurrence of optical anisotropy is observed at about 0.5 °C higher temperature when an electric field is applied.

when a higher voltage is applied above the isotropization temperature. At 120.8 °C (triangles) and 121 °C (inverted triangles), on the other hand, no noticeable change is observed over the entire voltage range measured. Here, we have to commit that the optical contrast between the 'on' and 'off' states is still not prominent even at 120.6 °C, revealing a maximum transmittance of about 8. In addition, the temperature range exhibiting the induced birefringence is very narrow. The molecular symmetry of the SiLC molecules may be easily collapsed in a mixed state because of the inherent flexibility of the cyclic tetramethyltetrasiloxane ring and hexyl chains in spite of the strong anchoring effect. In this regard, the well-defined structure within a LC

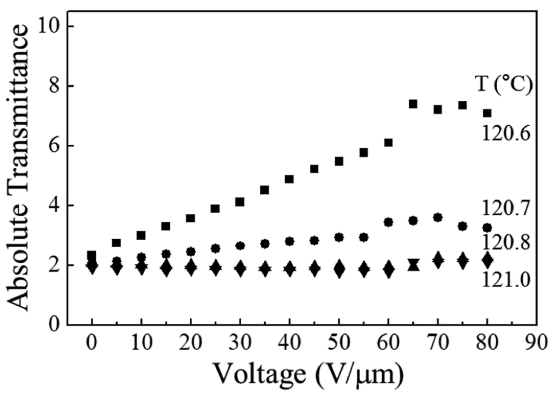

Fig. 9 The effect of electric field strength on the optical transmittance of the 80/20 SiLC/DiLC mixture. A rapid increase in the transmittance can be seen clearly upon increasing the voltage close to the isotropization temperature.

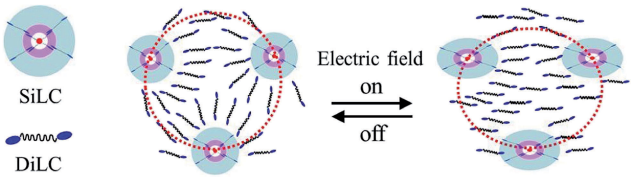

Fig. 10 A schematic illustration of the electric field-induced molecular alignment in the SiLC/DiLC system.

medium is not conserved well. The organic–inorganic hybrid materials having high symmetry along with proper rigidity may be idealistic to achieve the optically isotropic LC phase.

According to the constructed phase diagram, the mixture containing 80 wt% SiLC undergoes the phase transformations of (SmA_1 + Cr_2)–(L_1 + Cr_2)–(I) with increasing temperatures. In a voltage-off state, the long-range N order of the DiLC is effectively disturbed by the SiLC molecular surfactants, but the local molecular orientational order is conserved even above the isotropization temperature. The rod-shaped cyanobiphenyl mesogenic groups attached to SiLC and DiLC are susceptible to the external electric field due to its dipolar nature, which in turn organize the macroscopic nematic-like domain with the long-range molecular orientational order. The effect of an electric field on molecular assembly has been proposed in Fig. 10. The SiLC molecular surfactants containing high symmetry with four mesogenic arms at an 'off' state switch to an ellipsoidal shape at an 'on' state because of the preferential alignment of the mesogenic moieties parallel to the electric field. Since the short-range order within a finite size and responsive mobility of the LC medium is mainly influenced by the compositions, there exists an optimal blending composition.

4. Conclusions

The feasibility of electric field-induced birefringence in mixtures of the star-shaped liquid crystal (LC) molecular surfactants (SiLC) and the rod-shaped twin LC (DiLC) host molecules has been examined on the basis of the constructed phase diagram. The mixtures revealed various single and coexistence regions such as smectic A (SmA_1), nematic (N_2), crystal (Cr_2), smectic A + crystal (SmA_1 + Cr_2), liquid + crystal (L_1 + Cr_2), and liquid + nematic (L_1 + N_2) depending on the temperature and composition. The phase boundaries of the single and coexistent regions have been clarified by conducting the theoretical calculation. The validity of the constructed phase diagram was further verified by monitoring the morphological and structural evolution using cross-polarized optical microscopy and wide-angle X-ray diffraction techniques. Even though the magnitude of the induced birefringence under the AC electric field was not significant, the optical contrast between an isotropic state and an anisotropic state was clearly identified above the isotropization temperature. It is attributable to the formation of the macroscopic intermolecular order generated by the local reorientation of LC directors. The DiLC molecules may be successfully anchored on the SiLC molecular surfactants, but the molecular symmetry

of the SiLC molecules is easily collapsed because of the inherent flexibility of the cyclic tetramethyltetrasiloxane ring and methylene groups. The organic–inorganic hybrid giant LC surfactants with high symmetry and proper rigidity can allow us to form the stable optically isotropic LC phase in a wide temperature region.

Acknowledgements

This work was mainly supported by Basic Science Research (2013R1A1A2007238), KIST institutional program (2Z04320), and BK21 Plus program, Korea. D.-Y. Kim appreciates the support from Global Ph.D. Fellowship Program.

Notes and references

1 J. Kerr, *Philos. Mag.*, 1875, **50**, 337.
2 P. G. de Gennes and J. Prost, *The Physics of Liquid Crystals*, Oxford Sci., London, 1993.
3 P. G. de Gennes, *Mol. Cryst. Liq. Cryst.*, 1971, **12**, 193.
4 H. Khoshsima, H. Tajalli, A. Ghanadzadeh and R. Dabrowski, *J. Phys. D: Appl. Phys.*, 2006, **39**, 1495.
5 J. H. Jung, S.-E. Kim, E. K. Song, K. S. Ha, N. Kim, Y. Cao, C.-C. Tsai, S. Z. D. Cheng, S. H. Lee and K.-U. Jeong, *Chem. Mater.*, 2010, **22**, 4798.
6 S. H. Lee, S. S. Bhattacharyya, H. S. Jin and K.-U. Jeong, *J. Mater. Chem.*, 2012, **22**, 11893.
7 S. Meiboom, J. P. Sethna, W. P. Anderson and W. F. Brinkman, *Phys. Rev. Lett.*, 1981, **46**, 1216.
8 H. Kikuchi, M. Yokota, Y. Hiskado, H. Yang and T. Kajiyama, *Nat. Mater.*, 2002, **1**, 64.
9 Y. Hisakado, H. Kikuchi, T. Nagamura and T. Kajiyama, *Adv. Mater.*, 2005, **17**, 96.
10 Y. Haseba, H. Kikuchi, T. Nagamura and T. Kajiyama, *Adv. Mater.*, 2005, **17**, 2311.
11 Y. Haseba and H. Kikuchi, *J. Soc. Inf. Disp.*, 2006, **14**, 551.
12 S. W. Choi, S. I. Yamamoto, Y. Haseba, H. Higuchi and H. Kikuchi, *Appl. Phys. Lett.*, 2008, **92**, 043119.
13 M. Jiao, Y. Li and S. T. Wu, *Appl. Phys. Lett.*, 2010, **96**, 011102.
14 H. Yoshida, A. Takeda, Y. Taniguchi, Y. Tasaka, S. Kataoka, Y. Nakanishi, Y. Koike and K. Okamoto, *Mol. Cryst. Liq. Cryst.*, 2004, **410**, 255.
15 M. Oh-e and K. Kondo, *Appl. Phys. Lett.*, 1995, **67**, 3895.
16 D.-Y. Kim, S. Kim, S.-A. Lee, Y.-E. Choi, W.-J. Yoon, S.-W. Kuo, C.-H. Hsu, M. Huang, S. H. Lee and K.-U. Jeong, *J. Phys. Chem. C*, 2014, **118**, 6300.
17 J. Yamamoto and H. Tanaka, *Nature*, 2001, **409**, 321.
18 S. Kim, S.-W. Kang and K.-U. Jeong, *Soft Matter*, 2012, **8**, 9761.
19 D.-Y. Kim, P. Nayek, S. Kim, K. S. Ha, M. H. Jo, C.-H. Hsu, Y. Cao, S. Z. D. Cheng, S. H. Lee and K.-U. Jeong, *Cryst. Growth Des.*, 2013, **13**, 1309.
20 D.-Y. Kim, S.-A. Lee, Y.-J. Choi, S.-H. Hwang, S.-W. Kuo, C. Nah, M.-H. Lee and K.-U. Jeong, *Chem.–Eur. J.*, 2014, **20**, 5689.
21 D. Y. Kim, M. Park, S. A. Lee, S. E. Kim, C. H. Hsu, N. I. Kim, S. W. Kuo, T. H. Yoon and K. U. Jeong, *Soft Matter*, 2015, **11**, 58.
22 P. Dayal, R. A. Matkar and T. Kyu, *J. Chem. Phys.*, 2006, **124**, 224902.
23 P. J. Flory, *Principles of Polymer Chemistry*, Cornell University Press, New York, 1953.
24 M. L. Huggins, *J. Am. Chem. Soc.*, 1942, **64**, 1712.
25 W. Maier, *Z. Naturforsch., A: Astrophys., Phys. Phys. Chem.*, 1959, **14**, 882; W. Maier and A. Saupe, *Z. Naturforsch., A: Astrophys., Phys. Phys. Chem.*, 1960, **15**, 287.
26 H.-W. Chiu and T. Kyu, *J. Chem. Phys.*, 1995, **103**, 7471.
27 W. L. McMillan, *Phys. Rev. A*, 1971, **4**, 1238.
28 H.-W. Chiu and T. Kyu, *J. Chem. Phys.*, 1998, **108**, 3249.
29 P. R. Harrowell and D. W. Oxtoby, *J. Chem. Phys.*, 1987, **86**, 2932.
30 R. A. Matkar and T. Kyu, *J. Phys. Chem. B*, 2006, **110**, 12728.
31 R. Koningsveld, W. H. Stockmayer and E. Nies, *Polymer Phase Diagrams: A Textbook*, Oxford University, New York, 2001.
32 C. T. Imrie and G. R. Luckhurst, *Handbook of Liquid Crystals*, ed. D. Demus, J. W. Gray, H. W. Spies and V. Vill, Wiley-VCH, New York, 1999.
33 C. T. Imrie and P. A. Henderson, *Curr. Opin. Colloid Interface Sci.*, 2002, **7**, 298.
34 C. T. Imrie and P. A. Henderson, *Chem. Soc. Rev.*, 2007, **36**, 2096.
35 G. A. Oweimreen and M. A. Morsy, *Thermochim. Acta*, 2000, **346**, 37.
36 H. Shen, K.-U. Jeong, H. Xiong, M. J. Graham, S. Leng, J. X. Zheng, H. Huang, M. Guo, F. W. Harris and S. Z. D. Cheng, *Soft Matter*, 2006, **2**, 232.
37 K.-U. Jeong, D.-K. Yang, M. J. Graham, Y. Tu, S.-W. Kuo, B. S. Knapp, F. W. Harris and S. Z. D. Cheng, *Adv. Mater.*, 2006, **18**, 3229.
38 S. Leng, L. H. Chan, J. Jing, J. Hu, R. M. Moustafa, R. M. V. Horn, M. J. Graham, B. Sun, M. Zhu, K.-U. Jeong, B. R. Kaafarani, W. Zhang, F. W. Harris and S. Z. D. Cheng, *Soft Matter*, 2010, **6**, 100.
39 K.-U. Jeong, B. S. Knapp, J. J. Ge, S. Jin, M. J. Graham, F. W. Harris and S. Z. D. Cheng, *Chem. Mater.*, 2006, **18**, 680.
40 P. Rathi, T.-M. Huang, P. Dayal and T. Kyu, *J. Phys. Chem. B*, 2008, **112**, 6460.